Bioresource Technology 297 (2020) 122492

Contents lists available at ScienceDirect

Bioresource Technology

journal homepage: www.elsevier.com/locate/biortech

High performance of Mo-promoted Ir/SiO_2 catalysts combined with HZSM-5 toward the conversion of cellulose to C_5/C_6 alkanes

Lele Jin[a,b], Wenzhi Li[a], Qiying Liu[b], Longlong Ma[a,b], Chao Hu[c], Ajibola T. Ogunbiyi[a], Mingwei Wu[a], Qi Zhang[a,b,*]

[a] Laboratory of Basic Research in Biomass Conversion and Utilization, Department of Thermal Science and Energy Engineering, University of Science and Technology of China, Hefei 230026, PR China
[b] CAS Key Laboratory of Renewable Energy, Guangzhou Institute of Energy Conversion, Chinese Academy of Sciences, Guangzhou 510640, PR China
[c] School of Environment and Energy Engineering, Anhui Jianzhu University, Hefei 230601, PR China

ARTICLE INFO

Keywords:
Liquid fuel
Microcrystalline cellulose
Molybdenum
Hydrogenolysis

ABSTRACT

In this study, the Mo-promoted Ir/SiO_2 (Ir-MoO_x/SiO_2) catalysts combined with the zeolite HZSM-5 were used for the direct conversion of microcrystalline cellulose (MCC) to liquid fuel (C_5/C_6 alkanes) in n-dodecane/H_2O system. A synergistic effect was formed between the partially reduced MoO_x species and the Ir particles, which effectively promoted the catalytic activity of Ir/SiO_2 catalyst. When the Mo/Ir molar ratio was 0.5, a high yield of C_5/C_6 alkanes (91.7%) was achieved at 210 °C for 12 h. In addition, the main component of C_5/C_6 alkanes was n-hexane, which was proven to be obtained by the hydrogenolysis of the key intermediate, sorbitol, formed from the hydrolysis and hydrogenation of MCC.

1. Introduction

Currently, with the increased concerns about global warming and environmental pollution, more and more attention has been paid to the exploration on the clean renewable resource as feedstock for energy fuels and chemicals (Chen et al., 2018; Chen et al., 2019; Gu et al., 2018; Li et al., 2019; Wang et al., 2017; Zhang et al., 2019). Cellulose is not only the most abundant source of biomass, accounting for about 34–50% of lignocellulose materials, but also is regarded as a promising substitute to fossil fuels for both fine chemicals and fuels (Jiang et al., 2019; Kumar et al., 2019; Lu et al., 2019). Unlike corn and starch, cellulose cannot be directly digested by human beings due to its complex structure with β-1, 4-glycosidic bonds of D-Glucose monomers. Thus its use will have no negative influence on food supplies (Jin et al., 2019; Ribeiro et al., 2017; Romero et al., 2016; Xi et al., 2013; Zhu et al., 2014). In the last few decades, various approaches have been developed for the valorization of cellulose, which can be converted into many kinds of platform compounds, high-value chemicals and fuels (such as sugars, sugar alcohols, polyols, 5-hydroxymethylfurfural, γ-valerolactone and hydrocarbons, etc.) by different chemical transformation (Han and Lee, 2012; Zhu et al., 2014; Zou et al., 2016). Especially, the production of C_5/C_6 alkanes was particularly attractive and potential because of its rich raw materials and low CO_2 emissions (Zhang et al., 2012).

Hence, a great deal of efforts have been made for the production of C_5/C_6 alkanes. There are detailed investigation in literature describing the production of new transportation biofuels from sugars, sugar alcohols and some platform molecules such as 5-hydroxymethylfurfural (HMF) and furfural (Li et al., 2017; Wang et al., 2019a; Zhang et al., 2018, 2019). For examples, Ni/HZSM-5 catalyst was applied for the formation of liquid alkanes (C_5-C_6) through sorbitol hydrogenation (Zhang et al., 2012, 2014). Ru/C was proposed for the production of the C_5/C_6 alkanes from acid biomass hydrolysate with a dual-bed aqueous catalytic system (Weng et al., 2016). The Ir-ReO_x/SiO_2 catalyst combined with HZSM-5 was also used for the conversion of sugar and sugar alcohol to liquid alkanes (Chen et al., 2013). However, study on direct conversion of cellulose to alkanes was still in its infancy, for reasons attributed to the occurrence of a series of sequential complex reactions including hydrolysis, hydrogenation, dehydration and hydrodeoxygenation during the whole conversion process. According to previous researches, there were two main reaction pathways of cellulose to liquid alkanes being proposed. (i) Tomishige and co-workers established one major pathway named the sorbitol route (Chen et al., 2013; Liu et al., 2014c, 2015b; Xia et al., 2016). It was believed that cellulose was firstly broken down into glucose (and some disaccharides or oligosaccharide) upon acid hydrolysis. The glucose was then rapidly

* Corresponding author at: Laboratory of Basic Research in Biomass Conversion and Utilization, Department of Thermal Science and Energy Engineering, University of Science and Technology of China, Hefei 230026, PR China.
E-mail address: zhangqi@ms.giec.ac.cn (Q. Zhang).

https://doi.org/10.1016/j.biortech.2019.122492
Received 9 October 2019; Received in revised form 22 November 2019; Accepted 24 November 2019
Available online 26 November 2019
0960-8524/

hydrogenated to sorbitol, which was the main intermediate towards n-hexane. (ii) Sels and co-workers (de Beeck et al., 2015) put forward a different route called the HMF route. In this route, HMF, generated from cellulose via consecutive hydrolysis, dehydration, isomerization, was the key intermediate, which can be transformed into gasoline alkanes under deep hydrodeoxygenation of HMF. It has been found that the selective removal of oxygen from cellulose, accompanied with C–O hydrogenolysis, was necessary to produce C_5/C_6 alkanes in both pathways (Chen et al., 2013; Liu et al., 2014c). Therefore, the catalytic system that can efficiently break C–O bonds without excessive C–C breakage was essential for the transformation of cellulose to C_5/C_6 alkanes.

In past researches, the transition metals such as Mo, W, V, Mn, Sn, Nb, Re have been used as promoters and modified catalysts such as Rh, Ru, Pt, Pd or Ir (Guan et al., 2014; Koso et al., 2009a; Li et al., 2014; Liu et al., 2014a; Pholjaroen et al., 2015). Among these, Mo has been proved to be a more effective additive that can be used in many reactions (Mizugaki et al., 2015; Wang et al., 2014b). In Mu et al's studies, the binary catalysts MoO_3 and supported Rh species were applied for the selective hydrogenolysis of tetrahydrofurfuryl alcohol to 1, 5-pentanediol. It was found the MoO_3 dissolved partially in the liquid phase and produced the active sites (H_xMoO_3) for the C-O bond breaking (Guan et al., 2014). According to Tomishige et al, compared with W and Re, the addition of Mo to Rh/SiO_2 promoted the formation of 1, 5-pentanediol from tetrahydrofurfuryl alcohol more significantly because of the synergy between the MoO_x and the Rh metal surface (Koso et al., 2009b). According to our previous work, Ir-VO_x/SiO_2 had excellent performance for the conversion of MCC to C_5/C_6 alkanes (Jin et al., 2019). Thus the molybdenum instead of vanadium modified Ir/SiO_2 catalyst was researched in this study. And it was further found that the Ir-MoO_x/SiO_2 catalyst was more active in the production of liquid C_5/C_6 alkanes from MCC conversion. Firstly, silica itself was weakly acidic with a large specific surface. The stronger interaction between Ir and partially reduced MoO_x species was expected via the electron transfer from Ir particles to partially reduced isolated MoO_x, leading to high activity of the catalyst.

Therefore, in this work, Mo modified Ir/SiO_2 catalyst combined with the zeolite HZSM-5 was used for the conversion of microcrystalline cellulose (MCC) to liquid alkanes in a biphasic system (n-dodecane + H_2O). To the best of our knowledge, there was no report about the use of Mo modified Ir/SiO_2 as a catalyst for the transformation of cellulose to C_5/C_6 alkanes.

2. Material and methods

2.1. Material

SiO_2 (100 ~ 200 mesh) was purchased from Qingdao Haiyang Chemical Co., Ltd. (Qingdao, China). $H_2IrCl_6{\cdot}H_2O$ (Ir ≥ 36%) and α-cellulose (90 μm) were bought from Aladdin (Shanghai, China). $(NH_4)_6Mo_7O_{24}{\cdot}4H_2O$ (≥99.0%) were provided by Sinopharm Chemical Reagent Co., Ltd. (Shanghai, China). The standard reagents including acetophenone (≥99.0%), D-glucose (≥99.0%), D-sorbitol (≥99.5%), isosorbide (> 98.0%), n-hexane (≥99.5%), 2-methylpentane (≥99.0), 3-methylpentane (≥99.0),n-pentane (≥99.5%), isopentane (> 98.0%), methylcyclopentane (≥99.5%), cyclohexane (≥99.9%), 1-hexanol(≥99.5%), 2-hexanol(98%), 3-hexanol (98%), 1-pentanol (≥99.5%), 2-pentanol (≥99%), 3-pentanol (≥99%), 5-hydroxymethylfurfural (HMF, 98.0%), 2, 5-dimethyltetrahydrofuran (DMTHF, mix of cis and trans, 96%), 2, 5-dimethylfuran (DMF, 99%) and the solvent n-dodecane (> 99.0%) were purchased from Aladdin (Shanghai, China). The standard gases including methane, ethane, propane and butane were provided by Nanjing Shangyuan Industrial Gas Factory (Nanjing, China). Above all, all the reagents in this study were used as received without further purification.

2.2. Preparation of catalyst

The catalysts Ir/SiO_2 and Ir-MoO_x/SiO_2 were prepared by sequential incipient wet impregnation method (Koso et al., 2012; Mizugaki et al., 2015; Wang et al., 2014a). 1 g of SiO_2 was firstly mixed with 15 mL of $H_2IrCl_6{\cdot}H_2O$ aqueous solution, then stirred at 75 ℃, 400 ramp/min for 6 h, dried at 120 ℃ for 12 h. After that, the obtained Ir/SiO_2 was immerged in 15 mL of the $(NH_4)_6Mo_7O_{24}{\cdot}4H_2O$ aqueous solution with the Mo/Ir molar ratio of 0 ~ 2, and then stirred at 75 ℃, 400 ramp/min for 6 h, dried at 120 ℃ for 12 h again. The theoretical Ir loading amount of the Ir-MoO_x/SiO_2 catalysts were 4 wt% and theoretical Mo/Ir molar ratio was range from 0 to 2. Besides, the MoO_x/SiO_2 catalyst was also prepared by sequential incipient wet impregnation method. 1 g of SiO_2 was immersed in 15 mL of the $(NH_4)_6Mo_7O_{24}{\cdot}4H_2O$ aqueous solution and then stirred at 75 ℃, 400 ramp/min for 6 h, dried at 120 ℃ for 12 h. The theoretical Mo content of MoO_x/SiO_2 catalyst was 1 wt% that was the same as the Mo content of 4 wt% Ir–MoO_x/SiO_2 (Mo/Ir = 0.5). Finally, all the catalysts were calcined at 500 ℃ for 3 h in air with a ramp rate of 2 ℃.

2.3. Experimental method

The experiment was performed in a 50 mL stainless steel autoclave. At first, 0.25 g of Ir/SiO_2 or Ir-MoO_x/SiO_2 catalyst was put into an autoclave together with a stirrer and 19 mL of deionized water and heated at 210 ℃ with 4 MPa H_2 for 3 h for the reduction pretreatment. The stirring rate was 250 ramp/min. After the pretreatment, the reactor cooled down and the hydrogen was removed. 0.1 g of HZSM-5 and 0.5 g of substrate with 8 mL of n-dodecane were added together into the autoclave. Then the mixture was divided into two layers, the upper and lower layers were n-dodecane and deionized water, respectively. After the reactor was sealed, the air content was purged with flushing hydrogen over three times. Then the reactor was pressurized with H_2 to an appropriated pressure (2 MPa ~ 8 MPa) and heated to a given temperature with a rate of 5 ℃/min under magnetic stirring at the speed of 700 ramp. When the reaction was ended, the reactor was firstly cooled to room temperature in air, and then cooled in ice bath. The gases were collected by gas bag. The remaining reaction solution was separated into aqueous and organic phases. At the same time, 0.1 g of acetophenone was added as an internal standard to the organic phase. The catalysts were recovered by filtration. The gas products were analyzed by gas chromatograph (GC–1960) equipped with stainless steel packed column (7% SE-30chromosorbGHF, 2 × 0.6 m × 2 mm), and the volume of the gas products were obtained by drainage method. The products in organic phase were analyzed by gas chromatography (Shimadzu GC-2010) with an Agilent HP-5 column (30 m × 0.32 mm × 0.25 μm) and a FID. The products in the aqueous phase were examined by HPLC (Waters 515) equipped with a Waters 2414 refractive index detector using a HPLC organic acid analysis column (300 mm × 7.8 mm); and a Waters 2489 ultraviolet detector using a Waters Symmetry C18 column (4.6 × 150 mm × 5 μm). The conversion and yields were calculated on the carbon basis and defined as follows:

$$\text{Conversion [\%]} = \text{(weight of reactant charged - weight of reactant after reaction) /weight of reactant charged} \times 100\%$$

$$\text{Yield of product [\%C]} = \text{(moles of product} \times \text{C atoms in product) /(moles of reactant charged} \times \text{C atoms in reactant)} \times 100\%$$

The conversion of MCC to C_5/C_6 alkanes was investigated by using the catalysts with diverse Mo/Ir molar ratios, different reaction hydrogen pressure, reaction temperatures and reaction times. All of the reactions were repeated three times to ensure the reproducibility of the experimental results.

2.4. Characterization

X-ray diffraction patterns (XRD, 2θ = 10°–90°) of various catalysts were recorded on a PHILIPS X-ray diffractometer (Netherlands) equipped with Cu Ka radiation source at 40 kV and 15 mA.

The Transmission electron microscope (TEM) photographs and energy dispersive X-ray (EDX) analysis were taken on a JEM 2011 instrument (JEOL, Japan). The sample powder was ultrasonically dispersed in ethanol and put on Cu grids for TEM observation.

The specific BET surface areas and pore volumes of samples were determined by N_2-physisorption at −196 ℃ (Tristar II 3020 equipment, Micromeritics, USA).

The H_2 temperature-programmed reduction (H_2-TPR) and the NH_3 temperature-programmed desorption (NH_3-TPD) were both carried out by using TPx chemisorption analyzer (Quantachrome Instruments, USA). As for the H_2-TPR, the catalysts was firstly pretreated by raising the furnace temperature from 25 ˚C to 400 ˚C at a rate of 10 ˚C/min under an Argon purge (Helium for NH_3-TPD) and then cooled to the initial temperature. Next, the furnace temperature was ramped to 1000 ˚C at a rate of 10 ˚C/min. At the same time, the carrier gas was replaced by 10% H_2/Ar (10% NH_3/He for NH_3-TPD).

The Pyridine-IR spectrums of samples were recorded on the Nicolet iS50 FT-IR Spectrometer (Nicolet, USA) using KBr disks. 12 mg of sample was first activated at 300 ˚C for one hour in vacuum and then subjected to pyridine adsorption at room temperature.

X-ray photoelectron spectroscopy (XPS) analysis was taken using a Thermo Scientific ESCALAB 250Xi device (Thermo-VG Scientific, UK).

3. Results and discussion

3.1. Characterization of catalysts

3.1.1. XRD pattern

From the XRD patterns of reduced Ir/SiO_2 and Ir-MoO_x/SiO_2 catalysts with various Mo/Ir molar ratios that all reduced at 200 ℃, it can be seen that a broad diffraction peak at 2θ = 22.1˚, which represented the amorphous phase of the SiO_2 support, and the other characteristic peaks at 40.9˚ and 47.3˚, which was due to the metallic Ir (Liu et al., 2014a,b). Besides, there was no other diffraction peak being observed. These phenomenon implied that 200 ℃ was enough for total reduction of Ir species to the metallic phase. At the same time, compared with the reduced Ir-MoO_x/SiO_2 (Mo/Ir = 0.5) catalyst, in the XRD curves of unreduced Ir-MoO_x/SiO_2 (Mo/Ir = 0.5) catalyst, there were also only two diffraction peaks of SiO_2 and IrO_2, indicating that the presence of the Ir species was in the form of IrO_2 before being reduced. In addition, no diffraction peaks of Mo or MoO_x were found from the XRD patterns of various Ir-MoO_x/SiO_2 catalysts or reduced/unreduced MoO_x/SiO_2, which indicated that the Mo species was well-dispersed on the catalyst. Furthermore, only diffraction peaks of SiO_2 and metallic Ir can be observed in the XRD pattern of the Ir-MoO_x/SiO_2 (Mo/Ir = 0.5) catalyst after reaction, in which there was no obvious difference with the fresh Ir-MoO_x/SiO_2 (Mo/Ir = 0.5) catalyst. This phenomenon indicated that the crystal phases of Ir-MoO_x/SiO_2 catalyst hardly changed after reaction.

3.1.2. BET analysis

The specific BET surface areas, pore volumes and average pore diameters of reduced Ir/SiO_2 and Ir-MoO_x/SiO_2 with various Mo/Ir molar ratios (from 0 to 2) were depicted in Table 1. The specific surface area of a bare SiO_2 support was 426.9 $m^2\ g^{-1}$ with a pore volume of 0.825 $cm^3\ g^{-1}$. After adding Ir species, the specific surface area decreased slightly. When the molybdenum was incorporated, it can be observed that the specific surface area and pore volumes of Ir-MoO_x/SiO_2 both increased with the Mo/Ir molar ratio rising. The specific surface area was over 460 $m^2\ g^{-1}$ when the Mo/Ir molar ratio was 0.13, 0.25 or 0.5, which implied the addition of appropriate amount of molybdenum would increase the specific surface area of the Ir-MoO_x/SiO_2 catalyst. However, with the further increase of molybdenum addition, there were obvious decline in specific surface area and pore volumes of the Ir-MoO_x/SiO_2 catalyst. Especially, when the Mo/Ir molar ratio over 1, the specific surface area and pore volumes of Ir-MoO_x/SiO_2 catalyst were both lower than those of the pure SiO_2, which possibly due to the overflow of supported molybdenum species onto the Ir-MoO_x/SiO_2 surface.

Table 1
Specific surface area, pore volume and average pore diameter of SiO_2 and Ir-MoO_x/SiO_2 with various Mo/Ir molar ratios.

Cat.	Mo/Ir molar ratio	S_{BET} ($m^2\ g^{-1}$)	V_p ($cm^3\ g^{-1}$)	d_p (nm)
SiO_2	–	426.9	0.825	7.531
Ir-MoO_x/SiO_2	0	414.2	0.836	7.769
	0.06	447.6	0.860	7.682
	0.13	460.7	0.861	7.477
	0.25	461.8	0.877	7.595
	0.5	460.6	0.871	7.560
	0.75	455.5	0.867	7.609
	1	406.1	0.785	7.734
	2	411.1	0.768	7.473

3.1.3. TEM images.

The particle size distribution and morphological images of fresh Ir/SiO_2 and Ir-MoO_x/SiO_2 with various Mo/Ir molar ratios (from 0 to 2) were examined by TEM. It can be found that the Ir particle was large in Ir/SiO_2 catalyst. With the addition of molybdenum, the Ir particle size was first decreased and then increased again. When the Mo/Ir molar ratio was 0.5, the Ir particle was smallest. These results proved that the addition of Mo species had a significant effect on the Ir particle size. At the same time, there was no obvious change occurred in the Ir-MoO_x/SiO_2 after reaction. In addition, no molybdenum particles were observed, indicating that the molybdenum was well dispersed in Ir-MoO_x/SiO_2 catalyst. The EDS spectra analysis of the Ir-MoOx/SiO_2 (Mo/Ir = 0.5) catalyst further revealed Mo species were uniformly dispersed on the SiO_2 carrier, which was consistent with the results of XRD analysis.

3.1.4. TPR profile

The active H_2 binding sites of Mo_x/SiO_2, Ir/SiO_2 and Ir-MoO_x/SiO_2 with various Mo/Ir molar ratios of 0.06, 0.13, 0.25, 0.5, 0.75, 1 and 2 were determined by the H_2 temperature-programmed reduction (H_2-TPR) and the results of H_2 consumption of the catalysts were listed in Table 2. The TPR pattern of Ir/SiO_2 catalyst exhibited a sharp reduction peak at around 200 ℃, which was due to the reduction of iridium species (Lin et al., 2013; Liu et al., 2014a). At the same time, according to the H_2 consumption area of this peak (414.9 μmol H_2/g_{cat}), the IrO_2 was completely reduced to metallic Ir. Compared with Ir/SiO_2 catalyst, the MoO_x/SiO_2 catalyst was difficult to be reduced. A broad reduction peak can be observed at 400 ~ 500 ℃ from the TPR profile of MoO_x/

Table 2
Active sites of Ir-MoO_x/SiO_2 with various Mo/Ir molar ratios.

Cat.	V/Ir molar ratio	Peak position (℃)		Active sites (μmol H_2/g_{cat})
		θ_1	θ_2	
Ir-MoO_x/SiO_2	0	198	–	414.9
	0.06	183	–	422.6
	0.13	194	–	443.0
	0.25	184	–	468.6
	0.5	180	–	508.0
	0.75	169	–	591.8
	1	191	489	865.2
	2	173	461	735.6
MoO_x/SiO_2	–	–	554	202.2

Table 3
Acidity of Ir-MoO_x/SiO_2 with various Mo/Ir molar ratios.

Cat.	Mo/Ir molar ratio	Acid site (mmol NH_3/g_{cat})[a]	Acid site (μmol Py/g_{cat})[b]
Ir-MoO_x/SiO_2	0	0.88	46.9
	0.06	1.48	54.3
	0.13	1.96	59.1
	0.25	1.97	53.4
	0.5	2.39	58.2
	0.75	2.21	37.6
	1	2.08	46.2
	2	1.61	31.4
Ir-MoO_x/SiO_2 after reaction	0.5	2.40	57.9

[a] Amount of desorbed ammonia was determined by NH_3-TPD.
[b] Amount of pyridine was determined by FTIR spectra of pyridine adsorbed and outgassed at 30 °C.

SiO_2 catalyst, usually attributed to the reduction of well dispersed polymolybdenum species. After addition of Mo to Ir/SiO_2 catalyst, the obtained bimetallic catalyst Ir-MoO_x/SiO_2 showed only one reduction peak in a low temperature region (below 200 °C) when the Mo/Ir molar ratio was below 1. In addition, the larger amount of H_2 consumption the Ir-MoO_x/SiO_2 catalyst corresponds to the partial reduction of MoO_3 to MoO_x in the valence of around 4 in addition to the total reduction of IrO_2. These results suggested that the reduction of MoO_3 with a low content in Ir-MoO_x/SiO_2 catalyst was evidently affected by the presence of Ir species that the MoO_3 can be partially reduced at a very low temperature. Such a promotion effect can be explained by the spillover of hydrogen species from Ir particles to the MoO_x species attached on them. It can be also found that when the Mo/Ir molar ratio was 1 or higher, another reduction peak appeared at around 500 °C, which was caused by the excessive addition of molybdenum species (MoO_x).

3.1.5. Acidity analysis

To investigate the effect of acidity on the catalytic activity, the surface acidity of the Ir-MoO_x/SiO_2 catalysts was examined by NH_3-TPD and Pyridine-IR adsorption. The total amount of acid sites determined by NH_3 desorption was illustrated in Table 3. From the result of NH_3-TPD, there was a wide peak appeared at 500 ~ 800 °C for the Ir/SiO_2 catalyst, which correspond to the strong acid site (Wang et al., 2019b). After loading Molybdenum, the new peaks (below 400 °C and over 800 °C) were formed, which can be due to some weak (or middle) and stronger acid site, respectively (Wang et al., 2019b). At the same time, it can be observed that the number of the acid sites identified by NH_3 adsorption was first increased and then decreased as the Ir/Mo molar ratio increased from 0.06 to 2. This phenomenon indicated that the addition of molybdenum acting as a Lewis acidic center would increase the acidity of the Ir-MoO_x/SiO_2 catalysts. However, the decrease in the amount of acid site with high molybdenum content could be attributed to the coverage of the original acid sites on the surface of the Ir-MoO_x/SiO_2 because of the excessive addition of molybdenum which have been demonstrated in the BET and TEM analyses discussed previously. To determine the type of acid sites, the Py-IR spectroscopy of the Ir-MoO_x/SiO_2 catalysts were further detected between 1400 ~ 1650 cm^{-1}. The reflection bond at 1450 cm^{-1}, 1580 cm^{-1} and 1600 cm^{-1} were all ascribed to the Lewis acid sites (Gu et al., 2019; Li et al., 2018; Wang et al., 2019b). In addition, only a tiny reflection bond at 1540 cm^{-1} observed was corresponding to the Bronsted acid site, which was almost negligible. These results demonstrated that most of the acid sites on the surface of Ir-MoO_x/SiO_2 catalysts belonged to Lewis acid sites, which were the dominant species of these catalysts. The amounts of Lewis acid obtained by the integral peak area at 1450 cm^{-1} according to Zhang et al. (Li et al., 2018) are depicted in Table 3. It was found that the amount of acid site detected by pyridine adsorption also first increased and then decreased with increase in molybdenum content, which was consistent with the phenomenon of NH_3 adsorption. Besides, the surface acidity of the Ir-MoO_x/SiO_2 (Mo/Ir = 0.5) after reaction was also examined by NH_3-TPD and Pyridine-IR adsorption. There was almost no change in the type and amount of acid sites of Ir-MoO_x/SiO_2 (Mo/Ir = 0.5) after reaction, which implied that the surface acidity of the Ir-MoO_x/SiO_2 catalyst was relatively stable.

3.1.6. XPS analysis

In order to further understand the interactions between Mo and Ir species, the chemical states and the surface properties of metal functions were studied by XPS. From the result, the Ir 4f XPS spectra of reduced Ir/SiO_2 and Ir-MoO_x/SiO_2 was investigated, in which the splitting of Ir 4f peak into $4f_{5/2}$ and $4f_{7/2}$ was due to the spin orbit coupling of the 4f orbital (Date et al., 2018). In case of the Ir/SiO_2 catalyst, there was no shift of binding energy of Ir 4f observed, where the standard binding energies of Ir^0 $4f_{5/2}$ and Ir^0 $4f_{7/2}$ were 60.9 and 63.9 eV, respectively (Date et al., 2018; Kotz et al., 1984; Lin et al., 2013). However, when the molybdedum was added to Ir/SiO_2 catalyst, the binding energies of Ir $4f_{5/2}$ and Ir $4f_{7/2}$ in Ir-MoO_x/SiO_2 catalyst increased. This suggested that there was an electron transfer from Ir atoms to partially reduced isolated MoO_x. It thus resulted in Ir species with deficient electrons and Mo with enriched electrons, confirming that the MoO_x could be partially reduced at low temperatures in the presence of Ir. Combining the results of XPS and TPR, the significantly improved catalytic activity of Ir-MoO_x/SiO_2 catalyst was due to the stronger interaction between Ir and partially reduced MoO_x species via the electron transfer from Ir particles to partially reduced isolated MoO_x, leading to high activity of Ir active species.

3.2. Effect of reaction conditions

3.2.1. Effect of various Mo/Ir molar ratio on yield of C_5/C_6 alkanes

The Ir-MoO_x/SiO_2 catalysts with different Mo/Ir molar ratio (0, 0.06, 0.13, 0.25, 0.5, 1 and 2) combined with the zeolite HZSM-5 were tested to investigate the effect of various amount of Mo addition to Ir/SiO_2 catalyst on the conversion of MCC to C_5/C_6 alkanes (Table 4). The reaction was carried out at 210 °C for 12 h. The products were C_5/C_6 alkanes (such as n-hexane, 2-methylpentane, 3-methylpentane isopentane and n-pentane), alcohols (such as 1-hexanol, 2-hexanol, 3-hexanol, 1-pentanol, 2-pentanol and 3-pentanol), cyclic ethers (such as 5-hydroxymethylfurfural, 2,5-dimethyltetrahydrofuran and 2,5-dimethylfuran), sugar alcohols (such as glucose, sorbitol, isosobide) and the C–C cracking products (such as methane, ethane, ethylene, propane, propylene, butane and butene) and cycloalkanes (such as methylcyclopentane, cyclohexane). The catalytic performance was mainly evaluated by the conversion of MCC and the yields of the targeted products (C_5/C_6 alkanes).

In Table 4, it can be observed that the Mo/Ir molar ratio had a significant influence on the yields of C_5/C_6 alkanes. The Ir/SiO_2 catalyst exhibited low yield (18.1%) in C_5/C_6 alkanes, and a large amount of by-products and intermediates such as methylcyclopentane, cyclohexane, alcohols (pentanols and hexanols) and sorbitol were produced (Table 4, entry 1). After adding molybdenum to the Ir/SiO_2 catalyst, the conversion of MCC were all increased. At the same time, the yield of C_5/C_6 alkanes also increased with increasing Mo/Ir molar ratio from 0 to 0.5 and reached a maximum at 0.5 (84.9%) (Table 4, entries 1–5), indicating that the Ir-MoO_x/SiO_2 had excellent performance for MCC conversion and C-O hydrogenolysis. Conversely, the C_5/C_6 alkanes yield decreased when the Mo/Ir molar ratio was over 0.5, and even a very low yield of C_5/C_6 alkanes (16.9%) was obtained as the Mo/Ir molar ratio rose to 2 (Table 4, entries 6–8). This result can be explained by the possibility that the excessive addition of molybdenum species to Ir/SiO_2 catalyst would cause deposition on the surface of the catalyst, block the pores and make the Ir particles larger, thus affecting the catalytic effect. An evidence of this was seen in the decline in specific surface area, and pore volume from BET. The increase of large Ir

Table 4
Effect of molybdenum content on Yield of C_5/C_6 alkanes.[a]

Entry	Mo/Ir molar ratio	Yield/C%											
		Conv.	C_5/C_6	C4	C3	C2	C1	CA	CE	ALC	Sorbitol	Iss	Glu
1	0	94.3	18.1	0.0	0.0	4.6	1.9	12.7	0.6	8.9	3.2	0.9	1.9
2	0.06	96.7	78.0	0.4	1.7	2.1	3.3	1.5	0.1	0.5	0.0	0.0	1.7
3	0.13	> 99.9	83.7	0.3	0.8	1.9	2.6	1.4	0.0	0.2	0.0	0.0	1.7
4	0.25	> 99.9	83.6	0.3	0.7	2.0	3.5	1.4	0.0	0.3	0.0	0.0	1.7
5	0.5	> 99.9	84.9	0.3	1.6	2.1	3.4	1.2	0.0	0.1	0.0	0.0	1.7
6	0.75	> 99.9	62.7	0.3	1.0	1.1	2.3	2.8	0.2	1.0	0.0	1.8	1.6
7	1	99.2	41.4	0.3	0.9	0.7	1.8	5.4	0.2	0.8	1.4	4.7	1.6
8	2	99.1	16.9	0.2	0.9	1.7	0.8	6.9	0.5	4.2	5.4	3.0	1.8

[a] C_5/C_6: n-pentane, n-hexane, 2-methylhexane and 3-methylhexane. C4, butane; C3, propane; C2, ethane; C1, methane. CA (Cycloalkanes): other hydrocarbons (methylcyclopentane and cyclohexane). CE (Cyclic ethers): 5-hydroxymethylfurfural (HMF), 2, 5-dimethyltetrahydrofuran (DMTHF) and 2, 5-dimethylfuran (DMF). ALC (Alcohols): 1-pentanol, 2-pentanol, 3-pentanol, 1-hexanol, 2-hexanol and 3-hexanol. Iss: isosorbide. Glu: glucose. Reaction conditions: Microcrystalline cellulose (0.5 g), H_2O (19 mL), n-dodecane (8 mL), catalyst (0.25 g), HZSM-5 (0.1 g), initial H_2 pressure (4 MPa), 210 ℃ and 12 h.

particles on the surface of the catalyst by TEM and the appearance of the new reduction peak of molybdenum species in H_2-TPR when the Mo/Ir molar ratio was over 0.5. These results demonstrated that there was a synergistic effect between iridium and molybdenum species on Ir-MoO_x/SiO_2 catalyst, which was responsible for the excellent performance of Ir-MoO_x/SiO_2.

3.2.2. Effect of reaction temperature on yield of C_5/C_6 alkanes

The effect of various reaction temperatures (190, 200, 210, 220 and 230 ℃) on the conversion of MCC to C_5/C_6 alkanes was investigated by taking Ir-MoO_x/SiO_2 (Mo/Ir molar ratio = 0.5) and HZSM-5 as the composite catalysts with the reaction time of 2 h, and the result was shown in Fig. 1. It can be seen that the conversion of MCC and the yield of the main products C_5/C_6 alkanes were both increased when the reaction temperature increased from 190 to 210 ℃. However, there was a decline in the yield of C_5/C_6 alkanes with further increase in reaction temperature. Besides, the total yield of by-products C1-C4 alkanes increased from the initial 3.5% to 9.1% with reaction temperature increased from 190 to 230 ℃. This phenomenon indicated that high temperatures promote the conversion of MCC, leading to high yields of C_5/C_6 alkanes. However, too high a temperature would exacerbate the occurrence of side reactions and the C–C bond cleavage, produce more gaseous alkanes and thus result in a decrease in the yield of C_5/C_6 alkanes.

3.2.3. Effect of reaction time on yield of C_5/C_6 alkanes

In order to explore the influence of reaction time on the conversion of MCC to C_5/C_6 alkanes, the experiments with various reaction time of 2, 3, 6, 12 and 24 h were manipulated by taking Ir-MoO_x/SiO_2 (Mo/Ir molar ratio = 0.5) and HZSM-5 as the composite catalysts at a temperature of 210 ℃. The results were shown in Fig. 2. It can be observed that the conversion of MCC increased as reaction time prolonged, and the MCC was converted almost completely when the reaction time extended to or over 12 h. This result illustrated that reaction time was a positive factor for MCC conversion. At the meanwhile, it can be found that the yield of C_5/C_6 alkanes increased from 26.5 to 84.9% when the reaction time increased from 2 to 12 h. With reaction time further prolonged, the target product C_5/C_6 alkanes had no obvious change, implying that a moderate reaction time of 12 h seemed more reasonable and was preferred for the production of C_5/C_6 alkanes. In addition, the yields of the by-products including C1-C4 alkanes and cycloalkanes (methylcyclopentane/cyclohexane) also increased with the reaction time extended. In particular, the yields of sorbitol and isosorbide both increased at first and then decreased with the reaction time prolonged, which can be explained by the possibility that sorbitol and isosorbide were the significant intermediates during the conversion of MCC to C_5/C_6 alkanes.

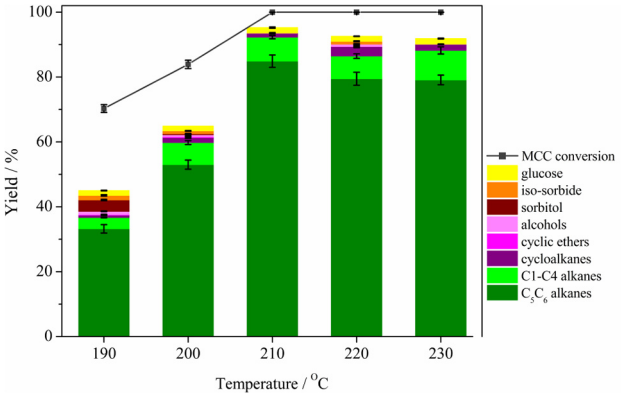

Fig. 1. Effect of reaction temperature. Reaction conditions: Microcrystalline cellulose (0.5 g), H_2O (19 mL), n-dodecane (8 mL), catalyst (0.25 g), HZSM-5 (0.1 g), initial H_2 pressure (4 MPa) and 12 h.

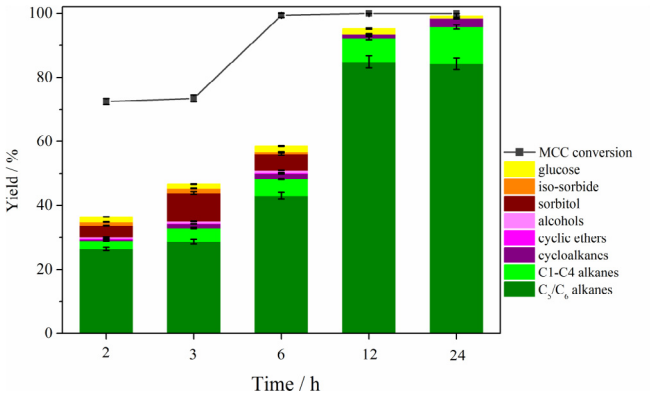

Fig. 2. Effect of reaction time. Reaction conditions: Microcrystalline cellulose (0.5 g), H_2O (19 mL), n-dodecane (8 mL), catalyst (0.25 g), HZSM-5 (0.1 g), initial H_2 pressure (4 MPa) and 210 ℃.

3.2.4. Effect of hydrogen pressure on yield of C_5/C_6 alkanes

For a better understanding of the reaction, the changes in the product yields were investigated with the hydrogen pressure varying from 2 to 8 MPa with the reaction temperature and time being fixed at 210 ℃ and 12 h by taking Ir-MoO_x/SiO_2 (Mo/Ir molar ratio = 0.5) and HZSM-5 as the composite catalysts. In Fig. 3, it can be seen the yield of C_5/C_6 alkanes increased dramatically from 57.0 to 84.9% when the H_2 pressure rose from 2 to 4 MPa. Then the C_5/C_6 alkanes yield continued to increase with hydrogen pressure increased, and a maximum yield of C_5/C_6 alkanes (91.7%) was obtained when the hydrogen pressure was

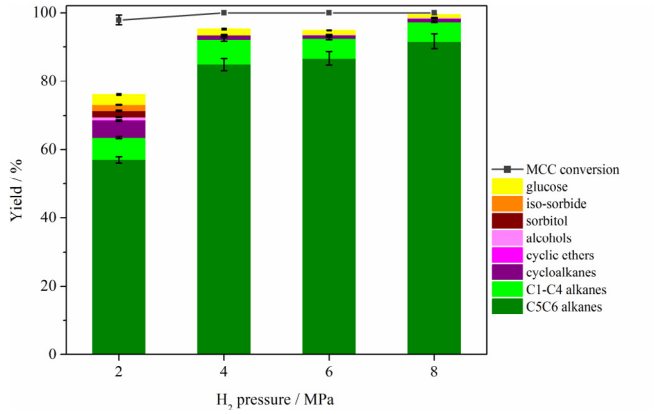

Fig. 3. Effect of hydrogen pressure. Reaction conditions: Microcrystalline cellulose (0.5 g), H_2O (19 mL), n-dodecane (8 mL), catalyst (0.25 g), HZSM-5 (0.1 g), 210 ℃ and 12 h.

8 MPa. Contrary to the yield of C_5/C_6 alkanes, there was a decline in yields of the by-products such as C1-C4 alkanes, methylcyclopentane and cyclohexane with the hydrogen pressure increased. This phenomenon can be explained by the increase of the hydrogen solubility in aqueous phase under high H_2 pressure. It would make the activation of hydrogen easier and inhibited the production of the by-products. Therefore, hydrogen pressure can promote the conversion of MCC to C_5/C_6 alkanes.

3.3. Reaction mechanism of cellulose to C_5/C_6 alkanes

In order to investigate the reaction pathway of MCC to C_5/C_6 alkanes, a series of experiments with various substrates (MCC, sorbitol, HMF, isosorbide, n-hexanol and n-pentanol) were conducted over Ir-MoO_x/SiO_2 combined with and without HZSM-5 at 210 ℃ for 2 h. According to previous research, it was believed that there were two pathways of cellulose to hexane via sorbitol or via 5-HMF (de Beeck et al., 2015; Liu et al., 2014c), thus the experiments with sorbitol and HMF as the substrate were carried out, in turn. It can be found that the yield of C_5/C_6 alkanes was 40.2% when sorbitol was used as the substrate, which was much higher than when 5-HMF was used as the substrate (9.1%) (Table 5, entries 4–5). This phenomenon implied the production of C_5/C_6 alkanes was mainly via sorbitol. Simultaneously, during the course of MCC conversion over Ir-MoO_x/SiO_2 combined with HZSM-5 (Fig. 2), plenty of sorbitol accumulated (8.9%) when the reaction time reached 3 h, indicating that sorbitol was a significant intermediate during the process of MCC conversion. Therefore, the sorbitol pathway was supported in this work. Generally, it was thought that cellulose was first hydrolyzed to soluble polysaccharide or glucose, which was then readily hydrogenated into sorbitol. Then n-hexane was obtained by the hydrogenolysis of sorbitol via sorbitan, isosorbide, hexanol, etc. At the same time, some pentane would be generated through decarboxylation of hexanols. For examples, there was 0.8% of pentane obtained when n-hexanol was used as the substrate (Table 5, 11-12).

In addition, it was noted that there was a large amount of methylcyclopentane/ cyclohexane (total yield of 20.5%) and 2, 5-dimethyltetrahydrofuran (DMTHF)/2, 5-dimethylfuran (DMF) (total yield of 8.2%) produced when 5-HMF was used as the substrate (Table 5, entry 5). At the same time, there was also a large amount of black solid residue formed during the process of HMF conversion. These facts demonstrated that the cycloalkanes (methylcyclopentane/cyclohexane) and cyclic ethers (DMTHF/ DMF) were mainly produced by the dehydration of glucose or isomerized fructose to 5-HMF and successive deoxyhydrogenation, hydrogenation and hydrolysis of the generated 5-HMF. Furthermore, as for the formation of C1-C4 alkanes, it have been validated that the C1-C4 alkanes can be produced by retro-aldol condensation (Liu et al., 2015a), decarbonylation (Li & Huber, 2010), or C–C hydrogenolysis of intermediates (de Beeck et al., 2015; Liu et al., 2014c; Liu et al., 2015b). It can be found that when MCC was taken as the substrate, there was 2.4% of C1-C4 alkanes produced, however, the yield of C1-C4 alkanes increased to 5.3% (Table 5, entry 1, 4). This result indicated that the C1-C5 alkanes were mainly formed by the hydrogenolysis of sorbitol. It can also be found that the conversion of n-hexanol to alkanes and the yields of n-hexane were 97.5% and 87.9%, respectively, when catalyzed by Ir-MoO_x/SiO_2 combined with and without HZSM-5 (Table 5, entries 8–9). This indicated that the addition of HZSM-5 could promote the hydrogenolysis activity of Ir-MoO_x/SiO_2 catalyst.

4. Conclusions

The composite catalysts Ir-MoO_x/SiO_2 and HZSM-5 were effective in the MCC conversion to C_5/C_6 alkanes. A maximum yield of 91.7% of C_5/C_6 alkanes was achieved under the optimal conditions. The doping of molybdenum greatly promotes the hydrogenation activity of Ir-MoO_x/SiO_2 catalyst, which can be explained by the spillover of hydrogen species from Ir particles to the MoO_x species. Besides, the

Table 5
Conversion of various substrates over Ir-MoO_x/SiO_2 combined with and without HZSM-5.[a]

Entry	Cat.	Sub.	Conv. (%)	Yield (%)											
				iso-pen	n-pen	n-hex	iso-hex	Sum (C_5/C_6)	C1-C4	CA	ALC	CE	Sorbitol	Iss	Glu
1	IrMo + HZSM-5	MCC	72.5	0.9	1.8	22.3	1.5	26.5	2.4	0.5	0.5	0.3	3.6	0.1	1.6
2	IrMo	MCC	25.9	0.2	0.4	1.5	0.1	2.2	1.9	0.1	3.1	0.1	0.1	1.3	1.5
3	HZSM-5	MCC	72.7	0.0	0.0	0.1	0.0	0.1	0.0	0.0	0.0	0.1	0.0	0.0	3.6
4	IrMo + HZSM-5	sorbitol	93.3	1.3	2.2	33.9	2.8	40.2	5.3	1.8	0.8	0.0	–	3.5	0.0
5	IrMo + HZSM-5	5-HMF	> 99.9	0.0	0.2	5.5	0.4	9.1	0.1	20.5	8.2[b]	2.4	–	–	8.9[c]
6	IrMo	sorbitol	84.8	0.1	0.3	1.7	0.1	2.2	4.3	0.1	1.7	0.0	–	5.1	0.0
7	HZSM-5	sorbitol	21.9	0.0	0.7	0.1	0	0.8	0.6	0.0	0.0	–	–	–	0.0
8	IrMo + HZSM-5	1-HxOH	> 99.9	0.0	0.8	97.5	0.2	98.5	0.8	0.0	0.2[d]	–	–	–	–
9	IrMo	1-HxOH	90.1	0.0	0.9	87.9	0.0	88.8	0.7	0.0	0.0	–	–	–	–
10	IrMo + HZSM-5	1-PeOH	> 99.9	0.0	84.6	0.0	0.0	84.6	0.2	0.0	0.0	–	–	–	–
11	Blank	MCC	19.4	0.0	0.0	0.0	0.0	0.0	0.0	0.0	0.0	0.0	0.0	0.0	1.7

[a] n-pen: n-pentane, n-hex: n-hexane, iso-hex: 2-methylhexane and 3-methylhexane. C1-C4: methane, ethane, propane, butane; CA (Cycloalkanes): other hydrocarbons (methylcyclopentane and cyclohexane). CE (Cyclic ethers): 5-hydroxymethylfurfural (HMF), 2, 5-dimethyltetrahydrofuran (DMTHF) and 2, 5-dimethylfuran (DMF). ALC (Alcohols): 1-pentanol (1-PeOH), 2-pentanol, 3-pentanol, 1-hexanol (1-HxOH), 2-hexanol and 3-hexanol. Iss: isosorbide. Glu: glucose. Reaction conditions: substrates (0.5 g), H_2O (19 mL), n-dodecane (8 mL), catalyst (0.25 g) with or without HZSM-5 (0.1 g), initial H_2 pressure (4 MPa), 210 ℃ and 2 h. [b] CE (Cyclic ethers): 2, 5-dimethyltetrahydrofuran (DMTHF) and 2, 5-dimethylfuran (DMF). [c]black solid residue [d]ALC (Alcohols): 1-pentanol, 2-pentanol, 3-pentanol, 2-hexanol and 3-hexanol.

addition of HZSM-5 improves the hydrogenolysis activity of Ir-MoO_x/SiO_2 catalyst. Finally, it was considered that the liquid fuel was produced via sorbitol pathway: the key intermediate sorbitol was first produced from the hydrolysis/hydrogenation of MCC, and then to liquid alkanes.

CRediT authorship contribution statement

Lele Jin: Conceptualization, Methodology, Software, Validation, Investigation, Writing - original draft, Writing - review & editing. **Wenzhi Li:** Conceptualization, Formal analysis, Funding acquisition, Writing - review & editing. **Qiying Liu:** Formal analysis, Funding acquisition. **Longlong Ma:** Funding acquisition, Writing - review & editing. **Chao Hu:** Resources. **Ajibola T. Ogunbiyi:** Writing - review & editing. **Mingwei Wu:** Resources. **Qi Zhang:** Conceptualization, Supervision, Funding acquisition, Writing - review & editing.

Acknowledgements

This work is financially supported by the National Natural Science Foundation of China (51876209), the National Key Research and Development Program of China (2018YFB1501402), Strategic Priority Research Program of the Chinese Academy of Sciences (Grant No. XDA 21060101) and the Natural Science Foundation of Guangdong Province (2017A030308010).

Appendix A. Supplementary data

Supplementary data to this article can be found online at https://doi.org/10.1016/j.biortech.2019.122492.

References

Chen, K.Y., Tamura, M., Yuan, Z.L., Nakagawa, Y., Tomishige, K., 2013. One-pot conversion of sugar and sugar polyols to n-alkanes without C-C dissociation over the Ir-ReOx/SiO2 catalyst combined with H-ZSM-5. ChemSusChem 6 (4), 613–621.

Chen, X.F., Ma, X.Q., Peng, X.W., Lin, Y.S., Yao, Z.L., 2018. Conversion of sweet potato waste to solid fuel via hydrothermal carbonization. Bioresour. Technol. 249, 900–907.

Chen, Z., Bai, X.L., Lusi, A., Jacoby, W.A., Wan, C.X., 2019. One-pot selective conversion of lignocellulosic biomass into furfural and co-products using aqueous choline chloride/methyl isobutyl ketone biphasic solvent system. Bioresour. Technol. 289.

Date, N.S., Hengne, A.M., Huang, K.W., Chikate, R.C., Rode, C.V., 2018. Single pot selective hydrogenation of furfural to 2-methylfuran over carbon supported iridium catalysts. Green Chem. 20 (9), 2027–2037.

de Beeck, B.O., Dusselier, M., Geboers, J., Holsbeek, J., Morre, E., Oswald, S., Giebeler, L., Sels, B.F., 2015. Direct catalytic conversion of cellulose to liquid straight-chain alkanes. Energy Environ. Sci. 8 (1), 230–240.

Gu, J., Xin, Z., Tao, M., Lv, Y.H., Gao, W.L., Si, Q., 2019. Effect of reflux digestion time on MoO3/ZrO2 catalyst for sulfur-resistant CO methanation. Fuel 241, 129–137.

Gu, L., Li, B.L., Wen, H.F., Zhang, X., Wang, L., Ye, J.F., 2018. Co-hydrothermal treatment of fallen leaves with iron sludge to prepare magnetic iron product and solid fuel. Bioresour. Technol. 257, 229–237.

Guan, J., Peng, G.M., Cao, Q., Mu, X.D., 2014. Role of MoO3 on a rhodium catalyst in the selective hydrogenolysis of biomass-derived tetrahydrofurfuryl alcohol into 1,5-pentanediol. J. Phys. Chem. C 118 (44), 25555–25566.

Han, J.W., Lee, H., 2012. Direct conversion of cellulose into sorbitol using dual-functionalized catalysts in neutral aqueous solution. Catal. Commun. 19, 115–118.

Jiang, L.Q., Zheng, A.Q., Meng, J.G., Wang, X.B., Zhao, Z.L., Li, H.B., 2019. A comparative investigation of pyrolysis with enzymatic hydrolysis for fermentable sugars production fast from cellulose. Bioresour. Technol. 274, 281–286.

Jin, L., Li, W., Liu, Q., Ma, L., Li, S., Liu, Y., Zhang, B., Zhang, Q., 2019. Catalytic conversion of cellulose to C5/C6 alkanes over Ir-VOx/SO2 combined with HZSM-5 in n-dodecane/water system. Fuel Process. Technol. 196, 106161.

Koso, S., Furikado, I., Shimao, A., Miyazawa, T., Kunimori, K., Tomishige, K., 2009a. Chemoselective hydrogenolysis of tetrahydrofurfuryl alcohol to 1,5-pentanediol. Chem. Commun. 15, 2035–2037.

Koso, S., Ueda, N., Shinmi, Y., Okumura, K., Kizuka, T., Tomishige, K., 2009b. Promoting effect of Mo on the hydrogenolysis of tetrahydrofurfuryl alcohol to 1,5-pentanediol over Rh/SiO2. J. Catal. 267 (1), 89–92.

Koso, S., Watanabe, H., Okumura, K., Nakagawa, Y., Tomishige, K., 2012. Comparative study of Rh–MoOx and Rh–ReOx supported on SiO2 for the hydrogenolysis of ethers and polyols. Appl. Catal. B 111–112, 27–37.

Kotz, R., Neff, H., Stucki, S., 1984. Anodic iridium oxide-films – Xps-studies of oxidation-state changes and O-2-evolution. J. Electrochem. Soc. 131 (1), 72–77.

Kumar, V., Sharma, D.K., Bansal, V., Mehta, D., Sangwan, R.S., Yadav, S.K., 2019. Efficient and economic process for the production of bacterial cellulose from isolated strain of Acetobacter pasteurianus of RSV-4 bacterium. Bioresour. Technol. 275, 430–433.

Li, H.Y., Ma, H.Z., Liu, T., Ni, J., Wang, Q.H., 2019. An excellent alternative composite modifier for cathode catalysts prepared from bacterial cellulose doped with Cu and P and its utilization in microbial fuel cell. Bioresour. Technol. 289.

Li, M.X., Li, G.Y., Li, N., Wang, A.Q., Dong, W.J., Wang, X.D., Cong, Y., 2014. Aqueous phase hydrogenation of levulinic acid to 1,4-pentanediol. Chem. Commun. 50 (12), 1414–1416.

Li, N., Huber, G.W., 2010. Aqueous-phase hydrodeoxygenation of sorbitol with Pt/SiO2-Al2O3: Identification of reaction intermediates. J. Catal. 270 (48–59).

Li, W.Z., Dou, X.M., Zhu, C.F., Wang, J.D., Chang, H.M., Jameel, H., Li, X.S., 2018. Production of liquefied fuel from depolymerization of kraft lignin over a novel modified nickel/H-beta catalyst. Bioresour. Technol. 269, 346–354.

Li, W.Z., Zhu, Y.S., Lu, Y.J., Liu, Q.Y., Guan, S.N., Chang, H.M., Jameel, H., Ma, L.L., 2017. Enhanced furfural production from raw corn stover employing a novel heterogeneous acid catalyst. Bioresour. Technol. 245, 258–265.

Lin, W., Cheng, H., He, L., Yu, Y., Zhao, F., 2013. High performance of Ir-promoted Ni/TiO2 catalyst toward the selective hydrogenation of cinnamaldehyde. J. Catal. 303, 110–116.

Liu, C.W., Zhang, C.H., Liu, K.K., Wang, Y., Fan, G.X., Sun, S.K., Xu, J., Zhu, Y.L., Li, Y.W., 2015a. Aqueous-phase hydrogenolysis of glucose to value-added chemicals and biofuels: A comparative study of active metals. Biomass Bioenergy 72, 189–199.

Liu, S.B., Amada, Y., Tamura, M., Nakagawa, Y., Tomishige, K., 2014a. One-pot selective conversion of furfural into 1,5-pentanediol over a Pd-added Ir-ReOx/SiO2 bifunctional catalyst. Green Chem. 16 (2), 617–626.

Liu, S.B., Amada, Y., Tamura, M., Nakagawa, Y., Tomishige, K., 2014b. Performance and characterization of rhenium-modified Rh-Ir alloy catalyst for one-pot conversion of furfural into 1,5-pentanediol. Catal. Sci. Technol. 4 (8), 2535–2549.

Liu, S.B., Tamura, M., Nakagawa, Y., Tomishige, K., 2014c. One-Pot conversion of cellulose into n-hexane over the Ir-ReOx/SiO2 catalyst combined with HZSM-5. ACS Sustain. Chem. Eng. 2 (7), 1819–1827.

Liu, Y., Chen, L.G., Wang, T.J., Zhang, Q., Wang, C.G., Yan, J.Y., Ma, L.L., 2015b. One-pot catalytic conversion of raw lignocellulosic biomass into gasoline alkanes and chemicals over LiTaMoO6 and Ru/C in aqueous phosphoric acid. ACS Sustain. Chem. Eng. 3 (8), 1745–1755.

Lu, M.S., Li, J.B., Han, L.J., Xiao, W.H., 2019. An aggregated understanding of cellulase adsorption and hydrolysis for ball-milled cellulose. Bioresour. Technol. 273, 1–7.

Mizugaki, T., Nagatsu, Y., Togo, K., Maeno, Z., Mitsudome, T., Jitsukawa, K., Kaneda, K., 2015. Selective hydrogenation of levulinic acid to 1,4-pentanediol in water using a hydroxyapatite-supported Pt-Mo bimetallic catalyst. Green Chem. 17 (12), 5136–5139.

Pholjaroen, B., Li, N., Huang, Y.Q., Li, L., Wang, A.Q., Zhang, T., 2015. Selective hydrogenolysis of tetrahydrofurfuryl alcohol to 1,5-pentanediol over vanadium modified Ir/SiO2 catalyst. Catal. Today 245, 93–99.

Ribeiro, L.S., Delgado, J.J., Orfao, J.J.D., Pereira, M.F.G., 2017. Direct conversion of cellulose to sorbitol over ruthenium catalysts: Influence of the support. Catal. Today 279, 244–251.

Romero, A., Alonso, E., Sastre, A., Nieto-Marquez, A., 2016. Conversion of biomass into sorbitol: cellulose hydrolysis on MCM-48 and D-Glucose hydrogenation on Ru/MCM-48. Micropor. Mesopor. Mat. 224, 1–8.

Wang, M., Nie, K.L., Cao, H., Xu, H.J., Fang, Y.M., Tan, T.W., Baeyens, J., Liu, L., 2017. Biosynthesis of medium chain length alkanes for bio-aviation fuel by metabolic engineered Escherichia coli. Bioresour. Technol. 239, 542–545.

Wang, X.H., Li, H.L., Lin, Q.X., Li, R., Li, W.Y., Wang, X.H., Peng, F., Ren, J.L., 2019a. Efficient catalytic conversion of dilute-oxalic acid pretreated bagasse hydrolysate to furfural using recyclable ironic phosphates catalysts. Bioresour. Technol. 290.

Wang, Y.M., Hou, Y.L., Hao, X., Wang, Z.L., Zhu, W.C., 2019b. Effect of metal-doped VPO catalysts for the aldol condensation of acetic acid and formaldehyde to acrylic acid. RSC Adv. 9 (11), 5958–5966.

Wang, Z.Q., Li, G.Y., Liu, X.Y., Huang, Y.Q., Wang, A.Q., Chu, W., Wang, X.D., Li, N., 2014a. Aqueous phase hydrogenation of acetic acid to ethanol over Ir- MoOx/SiO2 catalyst. Catal. Commun. 43, 38–41.

Wang, Z.Q., Pholjaroen, B., Li, M.X., Dong, W.J., Li, N., Wang, A.Q., Wang, X.D., Cong, Y., Zhang, T., 2014b. Chemoselective hydrogenolysis of tetrahydrofurfuryl alcohol to 1,5-pentanediol over Ir-MoOx/SiO2 catalyst. J. Energy Chem. 23, 4427–4434.

Weng, Y.J., Qiu, S.B., Wang, C.G., Chen, L.G., Yuan, Z.Q., Ding, M.Y., Zhang, Q., Ma, L.L., Wang, T.J., 2016. Optimization of renewable C5 and C6 alkane production from acidic biomass hydrolysate over Ru/C catalyst. Fuel 170, 77–83.

Xi, J.X., Zhang, Y., Xia, Q.N., Liu, X.H., Ren, J.W., Lu, G.Z., Wang, Y.Q., 2013. Direct conversion of cellulose into sorbitol with high yield by a novel mesoporous niobium phosphate supported Ruthenium bifunctional catalyst. Appl. Catal. A-Gen. 459, 52–58.

Xia, Q.N., Chen, Z.J., Shao, Y., Gong, X.Q., Wang, H.F., Liu, X.H., Parker, S.F., Han, X., Yang, S.H., Wang, Y.Q., 2016. Direct hydrodeoxygenation of raw woody biomass into liquid alkanes. Nat. Commun. 7.

Zhang, L.X., Tian, L., Sun, R.J., Liu, C., Kou, Q.Q., Zuo, H.W., 2019. Transformation of corncob into furfural by a bifunctional solid acid catalyst. Bioresour. Technol. 276, 60–64.

Zhang, Q., Wang, T.J., Li, B., Jiang, T., Ma, L.L., Zhang, X.H., Liu, Q.Y., 2012. Aqueous phase reforming of sorbitol to bio-gasoline over Ni/HZSM-5 catalysts. Appl. Energ. 97, 509–513.

Zhang, Q., Wang, T.J., Xu, Y., Zhang, Q., Ma, L.L., 2014. Production of liquid alkanes by controlling reactivity of sorbitol hydrogenation with a Ni/HZSM-5 catalyst in water. Energ. Convers. Manage. 77, 262–268.

Zhang, T.W., Li, W.Z., An, S.X., Huang, F., Li, X.Z., Liu, J.R., Pei, G., Liu, Q.Y., 2018. Efficient transformation of corn stover to furfural using p-hydroxybenzenesulfonic acid-formaldehyde resin solid acid. Bioresour. Technol. 264, 261–267.
Zhu, W.W., Yang, H.M., Chen, J.Z., Chen, C., Guo, L., Gan, H.M., Zhao, X.G., Hou, Z.S., 2014. Efficient hydrogenolysis of cellulose into sorbitol catalyzed by a bifunctional catalyst. Green Chem. 16 (3), 1534–1542.
Zou, J., Cao, D., Tao, W.T., Zhang, S.Y., Cui, L., Zeng, F.L., Cai, W.J., 2016. Sorbitol dehydration into isosorbide over a cellulose-derived solid acid catalyst. RSC Adv. 6 (55), 49528–49536.